



# In-process closed-loop control for stabilising the melt pool temperature in selective laser melting

Volker Renken<sup>1</sup> · Axel von Freyberg<sup>1</sup> · Kevin Schünemann<sup>1</sup> · Felix Pastors<sup>2</sup> · Andreas Fischer<sup>1</sup>

Received: 31 July 2018 / Accepted: 26 April 2019 / Published online: 7 May 2019  
© The Authors 2019, corrected publication 2024

## Abstract

Additive manufacturing processes are gaining more importance in the industrial production of metal components, as they enable complex geometries to be produced with less effort. The process parameters used to manufacture a wide variety of components are currently kept constant and closed-loop controls are missing. However, due to the part geometry that causes varying heat flow to neighbouring powder and solidified sections or due to deviations in the atmosphere caused by fumes within the work area, there are changes in the melt pool temperature. These deviations are not considered by system control, so far. It is, therefore, advisable to measure the melt temperature with sensors and to regulate the process. This work presents an approach that enables fast process control of the melt pool temperature and combines a closed-loop control strategy with a feedforward approach. The control strategies are tested by proof-of-concept experiments on a bridge geometry and partly powder-filled steel plates. Furthermore, results of a finite element simulation are used to validate the experimental results. Combining closed-loop and feedforward control reduces the temperature deviation by up to 90%. This helps to prevent construction errors and increases the part quality.

**Keywords** Control · Simulation · Modelling · Additive manufacturing · Selective laser melting

## 1 Introduction

During the last years, additive manufacturing (AM) technologies have become more and more important for several industries, such as aviation, medical or automotive industries [19]. The reason is the flexibility of the process to create complex three-dimensional geometries combined with superior mechanical properties (e.g. high strength) of the metallic parts. Furthermore, between the idea of a new product and its realisation, short time-to-market constraints are possible. There are layer-based processes such as laser-based powder bed fusion (LPBF) or electron beam melting (EBM) and free-form processes with powder or wire feed systems, known as directed energy deposition (DED). LPBF, also known as selective laser melting exhibits the highest cooling rates after melting the metal powder leading to finest grain

size, while DED offers the lowest cooling rate [6]. Within these processes with solidification rates between 100 mm/s and 5000 mm/s, suitable alloys with adequate melting and solidification dynamics (e.g. ALSi10 Mg, TiAl6V4, CoCr or Inconel 718) are needed [3, 13].

Current control approaches work with constant parameters for scan speed and laser power in an open loop. The simulation of the process offers possibilities to optimise open-loop control strategies [17] or in combination with machine-learning approaches [2]. Due to the high runtime of finite element model (FEM) simulation, efficient models are needed to be applied within closed-loop control [22]. Here, a pragmatic approach based on enthalpy equations and the influence on evaporation phenomena is shown. Process parameter settings for laser power and scan speed are usually found by trial-and-error strategies that lead to extensive costs and increased consumption of raw material and energy input [12]. Sensors are used for monitoring to guarantee the process traceability and to affect process parameters for the next production period within post-process analysis [21]. Thus, usage of low coherence scanning interferometry sensors to adapt the scanning parameters has been shown [5] or optical imaging systems are used [7, 10, 11].

✉ Volker Renken  
ren@bimaq.de

<sup>1</sup> Bremen Institute for Metrology, Automation and Quality Science, University of Bremen, Linzer Str. 13, 28359 Bremen, Germany

<sup>2</sup> Aconity GmbH, Kaiserstr. 98, 52134 Herzogenrath, Germany

Closed-loop quality control strategies have been used in various technology fields (e.g. laser chemical machining [23]); however, the use of sensors for closed-loop control is still in research phase for metal AM technology. Feedback control has been implemented in a real-time control loop using a photodiode and stabilising the sensor signal at cubes and overhangs [4]. A simple control algorithm, based on pyrometer measurement and switching off the laser when exceeding a threshold temperature, leads not only to better hardness but also to increased production times [16]. For EBM, a successful manipulation of the grain size based on an infrared camera has been implemented by automated control steps [14]. Closed-loop control based on measuring the melt pool depth by low coherence interferometry and adapting the laser power has been shown for laser welding [9]. For laser cladding, the melting temperature could be stabilised by a control approach with pyrometer adjusting the laser power online in combination with a predictive controller [20]. However, the laser cladding has slower time constants compared to LPBF and control times in the order of milliseconds are sufficient. For LPBF, the scan speeds are above 1000 mm/s and lead to challenging time constraints. The melt pool can be characterised by its diameter of about 100  $\mu\text{m}$  [5, 7, 11] and a reasonable control reaction within a fraction of the melt pool diameter is needed. A control reaction within a quarter diameter of 25  $\mu\text{m}$  would require a control cycle time of about 25  $\mu\text{s}$  (for scan speed 1000 mm/s). A high-speed melt pool and laser power monitoring was realised by a pyrometer approach, which reaches measurement times of 10  $\mu\text{s}$  and aims to a closed-loop control time of 60  $\mu\text{s}$  [1]. So far, closed-loop control has not become part of market-related LPBF machines. It is still an open question if it is possible to react within sufficient short time frames through the whole control loop. Furthermore, the stabilisation effect on the melt pool temperature by feedback combined with feedforward methods needs to be investigated.

The aim of this work is to show the controllability of the LPBF process in principle by measuring temperature effects with a pyrometer and controlling the laser power in a closed-loop by fast field programmable gate array (FPGA) hardware. To this end, control strategies for a discrete analysis after building a vector, a layer or a whole part as well as for the in-process control will be developed and shown in Sect. 2. An FPGA offers the possibility to parallelise the calculation tasks and achieves shorter cycle times compared to conventional CPU technology with serial processing [15]. The high time constraints of 25  $\mu\text{s}$  for the complete control cycle are challenging. For a simple calculation, a single processor solution could meet these time constraints, but if an increased control complexity is required, the parallelized structure is an unbeatable advantage and reason for its choice. Furthermore, the measuring element that receives irradiation intensities from the process has a central role

for a successful in-process control and will be examined. The experimental setup for the following test scenarios is introduced in Sect. 3. Another question is which control accuracy can be achieved by applying different feedforward and feedback control strategies. For the in-process control approach, simulation studies and experiments are designed to show the timing constraints as well as the stabilisation effects. Experimental results and simulation work are shown in Sect. 4. In conclusion, the results are discussed in Sect. 5.

## 2 Control concept

Different control strategies for LPBF are possible depending on the available sensors and their time constants. Cascaded control strategies enable reacting within sensor-related time constants and in a discrete or continuous behaviour [18]. Both, in-process and discrete control setups are possible and can be integrated in a cascaded control structure as shown in Fig. 1. Different sensors are planned to be used within this approach. For fast values of radiation intensities a pyrometer and for estimation of the melt pool depth a topographic sensor based on low coherence interferometry will be used. For the slower investigation, aggregated values of these two sensors will be used in combination with camera information in visible as well as in infrared range. The outer cascades are discrete and get as input a data set with set points from the pre-processing unit or the next higher cascade. As highest cascade, the powder layer cascade is layer-discrete or section-discrete and is introduced to adapt the set point for the inner next cascade, which sets the values for one vector. A section is defined as one limited hatch area of one layer after division of the layer in the pre-processing. Between two layers, the temperature distribution or topographic sensor information is used to adapt the set points and control parameter for the next layer exposure. In the vector cascade, the procedure is identical with respect to one layer and its exposure. The set points for one vector will be compared with an analysed time series of measured radiation intensities and recalculated for the next vector. The set points for each time step will be transferred to the inner melt pool cascade. There, the intensity values will be used in-process to realise a closed-loop control of the melt pool temperature. Besides the intensity, it is also possible to measure the melt pool depth and use it for control. In this paper, an intensity measurement is used and the control is focused on the melt pool cascade.

The realisation of the melt pool cascade is shown in Fig. 2. The core of the controller consists of an FPGA with an analog to digital converter (ADC) interface and a digital to analog converter (DAC). The measurement input  $m$  is read via the ADC and compared to the predefined set point  $SP$  of that value resulting in a control error:

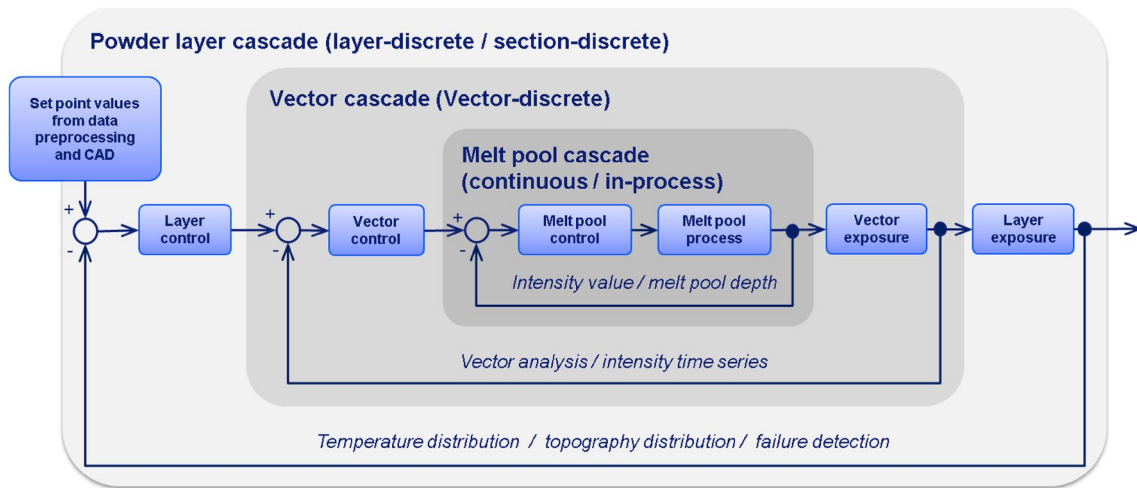


Fig. 1 Cascaded control structure with discrete and continuous behaviour

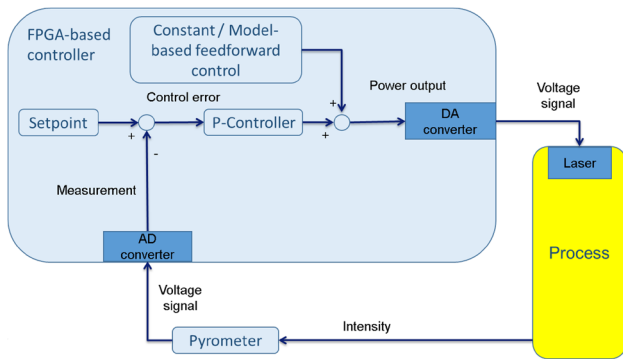


Fig. 2 Control structure of the melt pool cascade with respect to the used hardware

$$e = SP - m \tag{1}$$

The P-controller with the proportional constant  $k_p$  calculates a laser power output:

$$Laser_{out} = Laser_{in} + k_p \cdot e \tag{2}$$

from the control error  $e$  by adding either a constant basis value or a model-based feedforward value  $Laser_{in}$ . For the model-based approach, the constant feedforward value is changed stepwise in dependence of the expected thermal flow of the vector path.

Here, the constant  $Laser_{in}$  value is defined by conventional machine parameters for laser power of normal production settings. The set point  $SP$  was calculated from preliminary experiments analysing the pyrometer signal for proven process parameters. The proportional factor  $k_p$  was chosen to limit the laser power range to 25% of the maximal range. The process reacts on the physical laser power input as

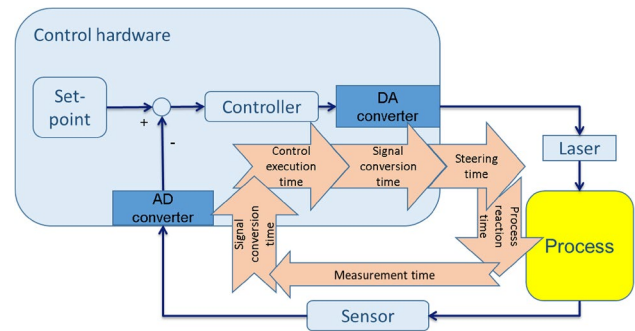


Fig. 3 Control time and its components in the control loop

manipulation parameter and sends out a temperature-based radiation back to the optical path of the machine. The temperature is used as control parameter. The pyrometer measures the radiation and forwards it as measurement parameter to the FPGA interface.

The control cycle time incorporates not only the application time of the controller itself, but also measuring time, signal-transmitting times, steering time and process delay time in the control loop (see Fig. 3).

In a preliminary reaction experiment, the response time of the whole control cycle is measured using three different signals. First, the  $Laser_{on}$  signal is transferred from the machine control system to the FPGA control board, second, the  $Laser_{out}$  signal of the FPGA board to the laser system and, finally, the pyrometer signal before transferring it as input signal to the FPGA. With these three signals, the control loop can be divided into two sub-loops. The first consists of the response time of the laser, the time constant of the process itself and the measurement time of the pyrometer. The second sub-loop consists of the signal conversion time

of the pyrometer signal or  $Laser_{on}$  signal to the FPGA board via ADC, the execution time of the FPGA and the signal conversion via DAC. The control time of the whole loop is the sum of both sub-loops. The times of the sub-loops are measured by inputting a step signal either by switching on the laser or by changing the laser on signal.

In Fig. 4a, the step response plots of the process (pyrometer output signal) and in Fig. 4b, of the controller (laser output signal) are given. For the process sub-loop, a reaction time of  $32\ \mu\text{s}$  is obtained. The used laser from type SPI red-POWER QUBE offers a rise time of  $5\ \mu\text{s}$  and has a general modulation frequency of  $20\ \text{kHz}$ . The sensor offers a time constant of less than  $10\ \mu\text{s}$ . For the controller reaction times of the FPGA board, the main part of the gathered time of  $13\text{--}14\ \mu\text{s}$  will be used for the signal conversion from analog to digital and vice versa. The FPGA controller itself works with a clock signal of  $50\ \text{MHz}$  and calculates the controller output by a simple P control algorithm within one cycle. Therefore, the execution time is below  $1\ \mu\text{s}$ . But, for the ADC, several clock signals are used. Thus, for ADC and DAC, a time constant of  $5\ \mu\text{s}$  each can be estimated.

The total control time is given by the sum of both the sub-loop constants of  $32\ \mu\text{s} + 14\ \mu\text{s} = 46\ \mu\text{s}$  and does not meet the preferable required control cycle time of  $25\ \mu\text{s}$ , but a reaction within half of the melt pool is achieved. Following on that, the chosen hardware is able to control the deviations of the temperature in the closed-loop for scan speeds  $\leq 1000\ \text{mm/s}$  and process stabilisation is realisable.

### 3 Experimental setup and test scenarios

To show the feasibility of controlling the melt pool temperature in-process, a number of proof-of-concept experiments have been designed to be conducted on an AconityMIDI LPBF machine (Aconity GmbH, Germany). The machine features a circular build platform with a diameter of  $170\ \text{mm}$  and employs a fibre laser combined with a 3D scanner system; see Fig. 5a. The build platform was open and the experiments have been carried in an air atmosphere. The laser is continuously steerable up to a laser power of  $500\ \text{W}$  with a production wavelength of  $\lambda_p = 1070\ \text{nm}$ . A high-speed pyrometer has been mounted on-axis into the optical path of the laser to observe the radiation intensities at operating point, see Fig. 5b.

The pyrometer Optris SN 8029001 measures intensities in the sensing wavelength range from  $\lambda_s = 850\ \text{nm} \dots 1000\ \text{nm}$ . It is important to block the laser wavelength within the optical path of the pyrometer to avoid fault measurements. Only the temperature-induced intensities can give a deduction on the temperature. Therefore, an additional filter in the laser wavelength of  $1070\ \text{nm}$  is used. The time constant of the pyrometer is below  $10\ \mu\text{s}$ . For the experiments in the next section, a gain factor is used with a characteristic output signal between  $0$  and  $5\ \text{V}$  corresponding to temperatures between  $750$  and  $1300\ ^\circ\text{C}$ . For sensor adjustment, a pilot laser in visible wavelength range is integrated into the sensor system and the overlap between spot sizes of working laser and sensor is maximised. The sensor fibre has a diameter of  $100\ \mu\text{m}$  and is connected via collimator to the optical path in rectilinear direction to the beam splitter.

With the described setup, three different experiments (bridge experiment, vector length experiment and powder

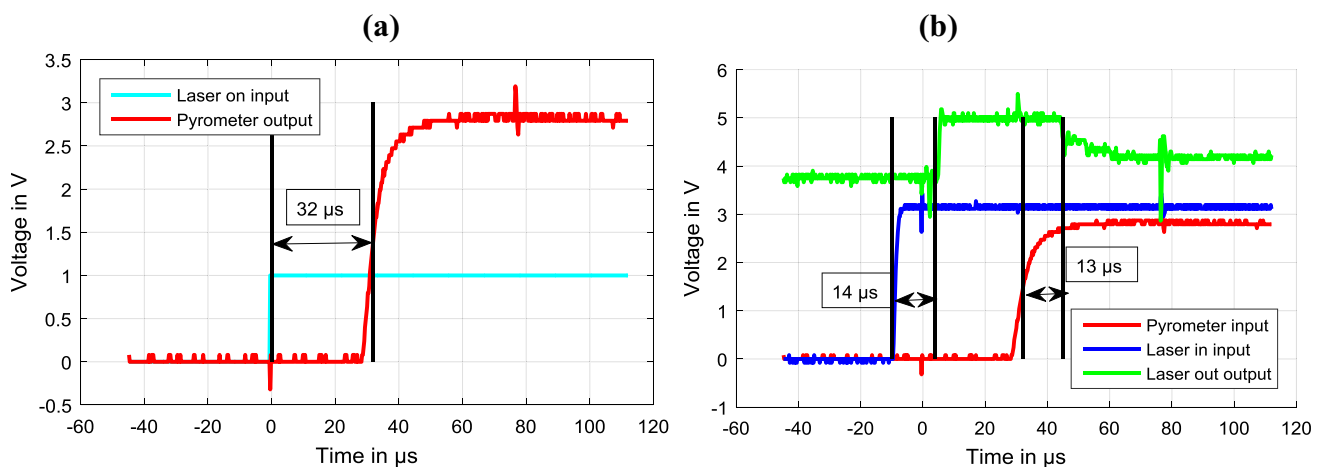


**Fig. 4** Reaction times of **a** the process after  $Laser_{on}$  signal and **b** the controller after  $Laser_{in}$  signal or after rising pyrometer signal. Note that the  $Laser_{on}$  signal is a digital signal that indicates the absolute

working time of the laser, while the  $Laser_{in}$  signal is an analog input from the machine that is measurable also before the working time of the laser

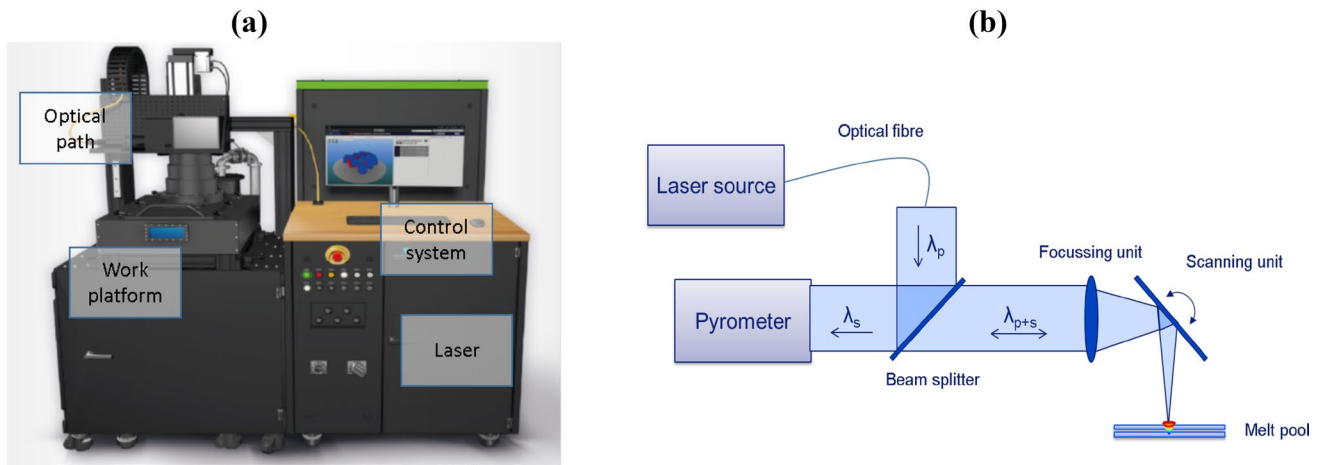


Fig. 5 The experimental setup with **a** the laboratory LPBF machine AconityMIDI from Aconity GmbH and **b** the optical path schematic

experiment) are conducted with varying test specimens or controller configurations. With the bridge experiment, a closed-loop and feedforward configuration is tested on geometry with changing heat flux and slow scan speed to test the controller strategies in principle. The vector length experiment has the aim to create a control task with changing heat levels and a realistic scan speed for open-loop and closed-loop configuration. The powder experiment realises the melting of powder at similar high scan speeds compared to the vector length experiment to evaluate the controller configuration for a powder-based control tasks. Table 1 presents a summary of the configuration setup for all experiments; see Sect. 4 for a detailed description. For all three experiments, the same control strategy, as shown in Sect. 2, was applied.

## 4 Experimental results and process modelling

### 4.1 Bridge experiment

The bridge experiment is conducted with a low scan speed and high energy input to generate large temperature gradients within the material and to enable secure power change points for the start of the bridge in model-based open-loop control mode. The control task is to stabilise the temperature of the melt pool that is detectable through the pyrometer signal. Four varying control strategies (“constant feedforward control”, “model-based feedforward control in two steps”, “closed-loop control” and “combined closed-loop and model-based feedforward control”) are applied. The strategy “model-based feedforward control in two steps” is a variation of the commonly used “constant feedforward control”. The only difference is that the signal to the laser is reduced, when higher temperatures appear in the simulation. Thus, in the bridge section, the laser power is reduced

Table 1 Overview of the experiments

Experiment	Specimen	Vector length, vector alignment	Controller configuration
Bridge experiment	Steel bridge with basis section (thickness = 8 mm) and bridge section (thickness = 0.5 mm)	10 mm per section, 6 adjacent parallel vectors with distance of 0.2 mm	Constant control, model-based control, closed-loop control and closed-loop combined with feedforward model-based control
Vector length experiment	Steel plate (thickness = 4 mm)	Filling quadratic areas with varying lengths of 2.5, 5 and 10 mm	Constant control and closed-loop control
Powder experiment	Steel plate (thickness = 8 mm) with solid section, followed by one-layer powder section and solid section	10 mm per section, 6 adjacent parallel vectors with distance of 0.2 mm	Constant control, model-based control, closed-loop control and closed-loop combined with feedforward model-based control



from 140 to 125 W. In the strategy “combined closed-loop and model-based feedforward control”, the same is done while closing the loop. Therefore, a feedback signal and a model-based varying feedforward signal are combined. The sum is then transferred to the laser hardware.

While scanning over a bridge structure with constant laser power, the temperature rises in the bridge section because of the limited heat flux to underlying regions of the specimen. Figure 6a shows the resulting pyrometer signals of the four controller configurations. It can be seen that for constant power of 140 W in combination with a slow scan speed of 10 mm/s, the part exhibits rising temperatures in the six bridge sections. For the last scan, the signal saturates at 3.7 V. In the closed-loop experiment with a P-controller, the deviation from the basic level is reduced and all six scans exhibit a similar step height. In the open-loop control mode, where the part is exposed with a laser power of 140 W in the basis section and of 125 W in the bridge section, the first two vectors show small deviation from the basic level. However, later scans show an increasing deviation. In the combined mode with closed-loop controller supported by the model-based feedforward control, the deviations are similar to

the closed-loop approach, but the average value of basis section is lower than in closed-loop mode.

In Fig. 6b, the heat effects on the specimen are presented. The high power input influences the neighbouring regions in the bridge section, but a visible difference between the control strategies cannot be detected. These differences can only be seen in the pyrometer signals. Table 2 shows the mean value and the standard deviation of the pyrometer signal for all four controller configurations. As a result, it can be seen that closed-loop control and combined closed-loop control with feedforward control achieve the best results, reducing the standard deviation by up to 90%. This demonstrates the benefit of using the pyrometer signal and a combination of closed-loop control and model-based feedforward control.

To validate the experiments, a finite element simulation is conducted on the bridge geometry from the experiments. To analyse the temperature development, there are five adjacent vectors with a length of 30 mm positioned over the bridge structure (see Fig. 7). Therefore, a 3D thermo-mechanical model was developed for the used geometry. The mesh grid is divided into two regions, to limit the simulation time. In the outer region with a distance around the defined vectors, where the energy input takes place,

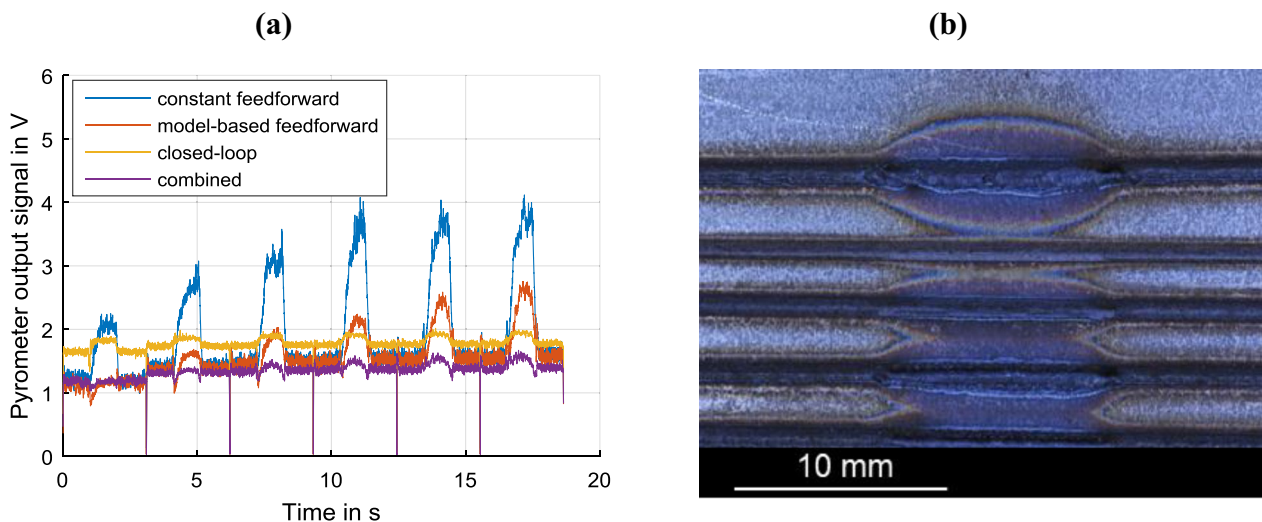


**Fig. 6** Bridge experiment with **a** pyrometer output signal and **b** the specimen after the laser exposure at “Laser in” with power  $P=140$  W scan speed  $v=10$  mm/s

**Table 2** Comparison between control strategies for bridge experiment

Experiment	Control Parameters	Mean pyrometer signal in V	Standard deviation in V
Constant feedforward control	$P=140$ W	1.90	0.66
Model-based feedforward control	$P=140$ W/125 W	1.55	0.23
Closed-loop control	$k_p=50$	1.78	0.07
Combining closed-loop control with feedforward control	$P=140$ W/125 W $k_p=50$	1.35	0.06

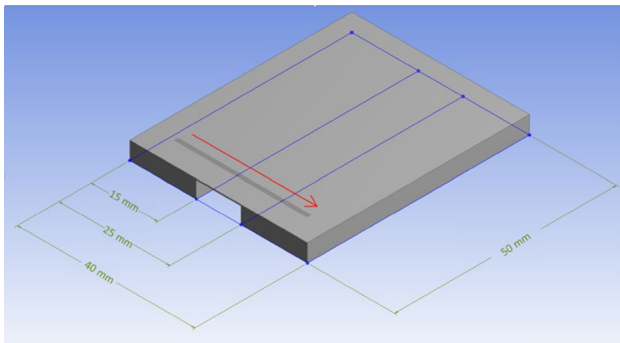


**Fig. 7** Dimensions of considered bridge geometry

a coarse net is used. In the region of the vectors, a mesh size with distances of 100  $\mu\text{m}$  between the nodes is used. In total, the simulation results in a number of 18,168 finite elements and 30,825 nodes. The time steps were chosen by the mesh size and the scan speed in a way, that one time step is simulated for each node while scanning the vectors. That leads to a frequency of 100 Hz for a scan speed of 10 mm/s. Within the simulation, an ambient temperature of 22  $^{\circ}\text{C}$  was defined and the part is thermally isolated to the surrounding volume. As part material, stainless steel with a density of 7750  $\text{kg}/\text{m}^3$ , a heat transfer coefficient of 15.1  $\text{W}/\text{m}^2\text{K}$  and a specific thermal capacity of 480  $\text{J}/\text{kg K}$  was chosen.

The results of the simulation can be evaluated in different ways. The main result of the simulation is the maximum temperature over time which can be used as the basis for different analysis. Figure 8a shows an exemplary temperature distribution while scanning over the bridge structure and the results of the maximum temperature development, it is notable that the temperature rises within the five scans and that the maximum of each scan is at the bridge (see Fig. 8b).

To analyse the influence of the scan speed and the laser power on the maximum temperature, different parameter

combinations (10, 20, 50, 100, and 1000 mm/s and 80, 160, 240, and 320 W) were applied, and the resulting maximum temperatures were compared.

In Fig. 9a, an almost linear increase of the maximum temperature for an increasing laser power is shown. The relation between the scan speed and the temperature shows a strongly increased temperature for slow scan speeds (see Fig. 9b).

To compare the influence of the parameters on the relative height of the steps, the quotient between the temperature on the bridge section and the temperature at the basis of the bridge is computed. Increasing the laser power has almost no influence on relative step height (see Fig. 10a). The relation between scan speed and relative step height shows a similar course as the maximum temperature (Fig. 10b). Thus, the most interesting influence on the maximum temperature and the temperature rise at the bridge is the scan speed.

Varying the process parameters in the experiments leads to indifferent results: in principle, the behaviour is similar, but due to the limited number of executed experiments with the given simulation circumstances, the shown effects cannot be completely confirmed. The exponential decreasing dependence of the temperature from the scan speed as shown in Fig. 9b is also recognizable in the experimental results after applying Planck's law for the calculation of the temperature from the pyrometer voltage. The same can be stated for the dependence shown in Fig. 10b, but the reduction of the bridge effect is greater. For example, the experimental coefficient for a scan speed of 50 mm/s is at a level of 1.02 compared to 1.12 in the simulation, while the quotient factor for a scan speed of 10 mm/s is similar to the simulation. That means in principle the simulation results confirm the experimental results, but further adaption of the models is required in future simulation development.

## 4.2 Vector length experiment

In this experiment, quadratic hatch areas with three different vector lengths (2.5, 5, and 10 mm) are exposed. By scanning

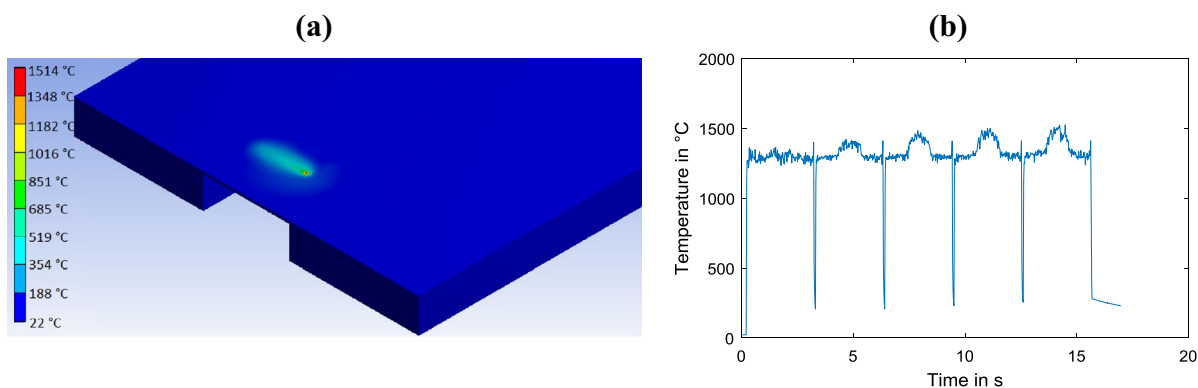


**Fig. 8** Simulation results as **a** temperature distribution while scanning over the bridge and **b** maximum temperature over time

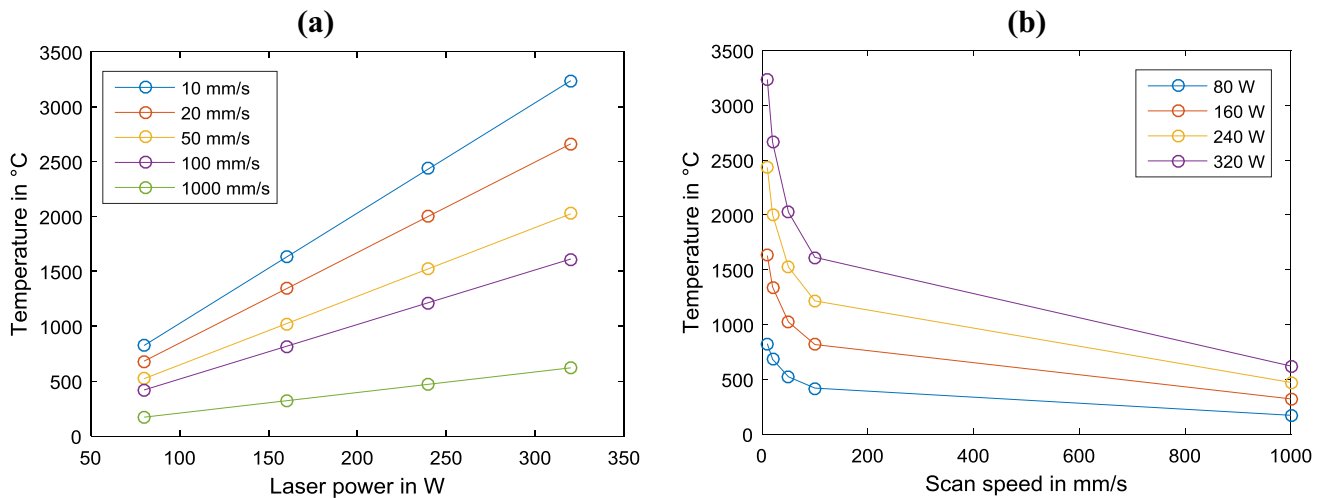


**Fig. 9** Simulation results for the maximum melt pool temperature by design of experiments, varying scan speed and laser power depending **a** on the laser power and **b** on the scan speed

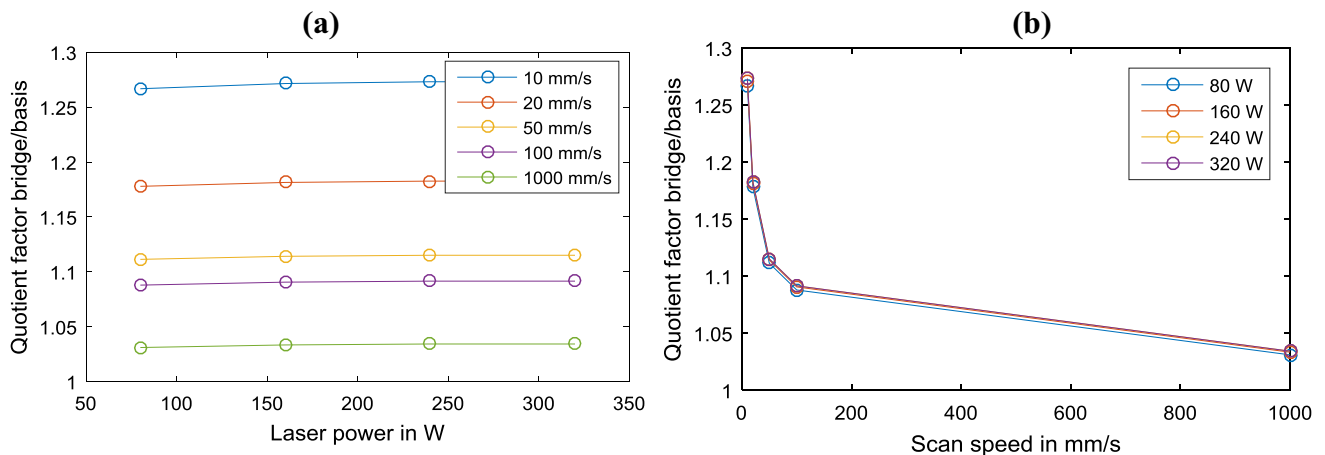


**Fig. 10** Investigation of influences on the quotient factor between bridge temperature and basis temperature from the process parameters **a** laser power and **b** scan speed

shorter vectors at constant scan speed of 800 mm/s, the cooling time between adjacent vectors is reduced and a higher temperature in this area is expected. An equalisation effect by applying the closed-loop controller will be investigated.

In Fig. 11a, the specimen after exposure is shown and Fig. 11b illustrates the pyrometer time series for vector lengths of 2.5 mm and 5 mm. The heat increase is clearly visible, especially for the short vector length region where the pyrometer signal exhibits a higher level than for longer vectors. Figure 11c shows mean pyrometer signals for the open-loop control with constant laser power of 190 W during laser exposure (cf.  $Laser_{on}$  signal in Fig. 11b). It can be seen that all vectors start with an overshoot in the beginning and also a rising signal in the end. In the middle region, a constant mean value is achieved. A typical vector

with 2 mm length has a higher middle level than the longer vectors, as expected. In Fig. 11d, the corresponding curves of the closed-loop control strategy are shown. The total level of the signal is higher in the closed-loop approach. That is why the set point was chosen at 0.6 V a little bit higher than the signals in constant laser power approach. The controller limits the height of the overshoots at the beginning and the end of the vector. Furthermore, the difference in the middle section between the single vectors is decreased from 0.093 V between 2.5 mm vector length and 10 mm vector length in open-loop case to 0.042 V in closed-loop case. Hence, the effect of process control is apparent, as the gap between the temperatures of different vector lengths can be reduced by over 50% between



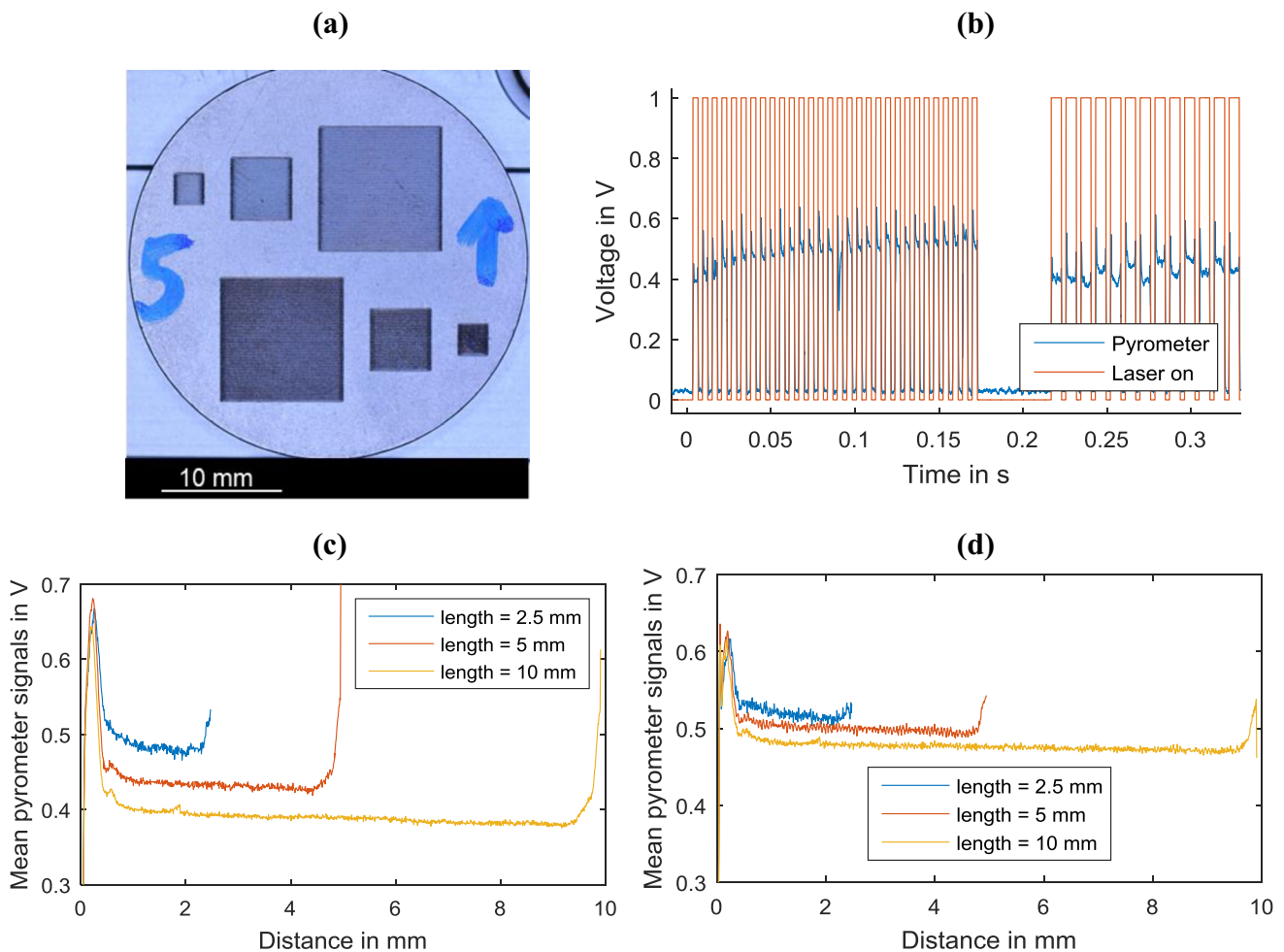


**Fig. 11** Vector length experiment **a** specimen and **b** pyrometer signal time series from two of the three vector lengths. The mean signals of all vectors with a specific length are shown for **c** the open-loop case and for **d** the closed-loop case. Powder experiment

open-loop and closed-loop strategy. Therefore, the control benefit is also given for higher scan speeds.

Here, the parameters are set to approach more realistic process settings. A powder layer is used in the middle section of the scans (see Fig. 12b), and the scan speed is increased to 600 mm/s. It can be seen that for constant power input, there is an effect similar to the bridge effect in the first experiment: the signal rises in the middle section of each scan vector (see Fig. 12a). Furthermore, the signal reaches its maximum during exposure of the first vector.

Calculating the standard deviation reveals that the single closed-loop approach achieves the best results reducing the standard deviation by nearly 70% compared to constant feedforward control (see Table 3). With the feedforward control approach, there are larger deviations, especially in the middle section. In general, the powder experiments exhibit larger standard deviations compared to the previous experiments without powder. This might be caused by the dynamic behaviour of the melting process of powder grains, due to

the complexity of the fundamental physics and dynamics of the LPBF process [8].

## 5 Conclusion

Due to deviations of environmental conditions, such as weld fumes or varying heat flux, constant open-loop parameters lead to limited quality of the built parts. Measuring the radiation intensities and deriving the temperature offers potential to solve this issue. In the reaction experiment, the suitability of the selected hardware and interfaces is shown. A whole-loop control time of 46  $\mu$ s is achieved in the preliminary experiment. The conducted proof-of-concept experiments prove the feasibility of in-process measurement and closed-loop control in less than half or the melt pool diameter. The model-based feedforward control optimises the results within the experiments.

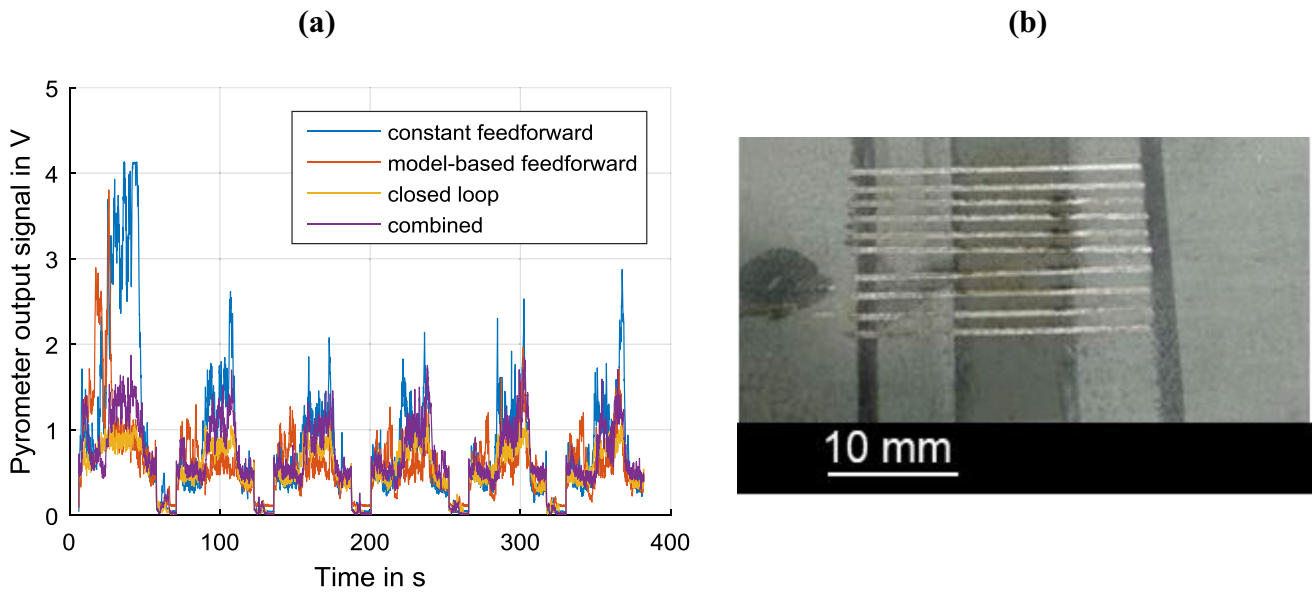


**Fig. 12** Powder experiment with **a** four controller configurations and **b** a picture of the exposed vectors

**Table 3** Comparison between control strategies for powder experiment

Experiment	Control parameters	Mean pyrometer signal in V	Standard deviation in V
Constant feedforward control	$P = 140 \text{ W}$	0.98	0.61
Model-based feedforward control	$P = 140 \text{ W}/125 \text{ W}$	0.69	0.315
Closed-loop control	$k_p = 50$	0.63	0.19
Combining closed-loop control with feedforward control	$P = 140 \text{ W}/125 \text{ W } k_p = 50$	0.76	0.308

In the bridge experiments, a decrease of the pyrometer signal's standard deviation by up to 90% can be achieved in comparison to an open-loop strategy with constant laser power application. Model-based open-loop control also reduces the deviations compared to the constant power approach. Combining model-based feedforward and feedback strategy leads to the lowest standard deviation of the pyrometer signal. In the vector length experiment, the effect of parameter variation in hatch areas is shown. An increase of the vector length leads to lower temperature in the vectors, due to the fact that the heat has more time to be dissipated to other regions of the sample part. The distance between the balanced temperature levels of the three vector lengths can be reduced by applying a closed-loop control. Furthermore, overshoot signals at the start and the end of each vector can be reduced by 50%. Within the powder experiments, the control ability is indicated for fast scan speeds of 600 mm/s and for the powder-melting process. The powder leads to higher standard deviations within the pyrometer measurement signal. Here, the model-based approach and the combined approach achieve a decrease of pyrometer signal standard deviation

in comparison to the constant feedforward control. However, in contrast to the bridge experiment, the simple closed-loop strategy leads to the best results, reducing the pyrometer standard deviation by about 70%.

In conclusion, closed-loop control of LPBF processes is a promising approach. The control ability is given by the used pyrometric and FPGA-based implementation, in principle. The feedback and model-based feedforward control strategies reduce the deviation of process temperature in the shown experiments which leads to more stable conditions in the melt pool. Next steps include incorporating the control strategy in realistic build processes in a closed build chamber with inert atmosphere. The models used in model-based feedforward control have to be optimised and generalised to arbitrary geometries to be applied in production jobs and control strategies in higher control cascades.

**Acknowledgements** This research was funded by the German Federal Ministry of Education and Research (BMBF) within the framework concept "Research for Tomorrow's Production" (project "In-process Sensors and adaptive control systems for additive manufacturing process", InSensa, fund number 02P15B076). On behalf of all the authors, the corresponding author states that there is no conflict of interest.

**Open Access** This article is licensed under a Creative Commons Attribution 4.0 International License, which permits use, sharing, adaptation, distribution and reproduction in any medium or format, as long as you give appropriate credit to the original author(s) and the source, provide a link to the Creative Commons licence, and indicate if changes were made. The images or other third party material in this article are included in the article's Creative Commons licence, unless indicated otherwise in a credit line to the material. If material is not included in the article's Creative Commons licence and your intended use is not permitted by statutory regulation or exceeds the permitted use, you will need to obtain permission directly from the copyright holder. To view a copy of this licence, visit <http://creativecommons.org/licenses/by/4.0/>.

## References

- Alberts D, Schwarze D, Witt G (2016) High speed melt pool & laser power monitoring for selective laser melting (SLM<sup>®</sup>). In 9th International conference on photonic technologies LANE, Fürth
- Baturynska I, Semeniuta O, Martinsen K (2018) Optimization of process parameters for powder bed fusion additive manufacturing by combination of machine learning and finite element method: a conceptual framework. *Procedia CIRP* 67(1):227–232
- Bourell D, Kruth JP, Leu M, Levy G, Rosen D, Beese AM, Clare A (2017) Materials for additive manufacturing. *CIRP Ann* 66(2):659–681
- Craeghs T, Bechmann F, Berumen S, Kruth J-P (2010) Feedback control of layerwise laser melting using optical sensors. *Phys Procedia* 5:505–514
- DePond PJ, Guss G, Ly S, Calta NP, Deane D, Khairallah S, Matthews MJ (2018) In situ measurements of layer roughness during laser powder bed fusion additive manufacturing using low coherence scanning interferometry. *Mater Des* 154:347–359
- Herzog D, Seyda V, Wycisk E, Emmelmann C (2016) Additive manufacturing of metals. *Acta Mater* 117:371–392
- Islam M, Purtonen T, Piili H, Salminen A, Nyrhilä O (2013) Temperature profile and imaging analysis of laser additive manufacturing of stainless steel. *Phys Procedia* 41:835–842
- King WE, Anderson AT, Ferencz RM, Hodge NE, Kamath C, Khairallah SA, Rubenchik AM (2015) Laser powder bed fusion additive manufacturing of metals; physics, computational, and materials challenges. *Appl Phys Rev* 2(4):041304
- Kogel-Hollacher M, Schoenleber M, Bautze T, Strebel M, Moser R (2016) Measurement and closed-loop control of penetration depth in laser materials processing. In: 9th international conference on photonic technologies LANE, Fürth
- zur Jacobsmühlen J, S Kleszczynski, D Schneider, G Witt (2013) High resolution imaging for inspection of laser beam melting systems. In: Instrumentation and measurement technology conference (I2MTC), 2013 IEEE International. IEEE
- Lane B, Moylan S, Whittenton EP, Li Ma (2016) Thermographic measurements of the commercial laser powder bed fusion process at NIST. *Rapid Prototyp J* 22(5):778–787
- Mani M, Lane BM, Donmez MA, Feng SC, Moylan SP (2017) A review on measurement science needs for real-time control of additive manufacturing metal powder bed fusion processes. *Int J Prod Res* 55(5):1400–1418
- Martin JH, Yahata BD, Hundley JM, Mayer JA, Schaedler TA, Pollock TM (2017) 3D printing of high-strength aluminium alloys. *Nature* 549(7672):365
- Mireles J, Terrazas C, Gaytan SM, Roberson DA, Wicker RB (2015) Closed-loop automatic feedback control in electron beam melting. *Int J Adv Manuf Technol* 78(5–8):1193–1199
- Monmasson E, Cirstea MN (2007) FPGA design methodology for industrial control systems—a review. *IEEE Trans Industr Electron* 54(4):1824–1842
- Nassar AR, Keist JS, Reutzel EW, Spurgeon TJ (2015) Intra-layer closed-loop control of build plan during directed energy additive manufacturing of Ti–6Al–4V. *Addit Manuf* 6:39–52
- Neugebauer F, Keller N, Ploshikhin V, Feuerhahn F, Köhler H (2014) Multi scale FEM simulation for distortion calculation in additive manufacturing of hardening stainless steel. In: Proc. Int. workshop on ‘thermal forming and welding distortion’, Bremen
- Renken V, Albinger S, Goch G, Neef A, Emmelmann C (2017) Development of an adaptive, self-learning control concept for an additive manufacturing process. *CIRP J Manuf Sci Technol* 19:57–61
- Schmidt M, Merklein M, Bourell D, Dimitrov D, Hausotte T, Wegener K, Overmeyer L, Vollertsen F, Levy GN (2017) Laser based additive manufacturing in industry and academia. *CIRP Ann* 66(2):561–583
- Song L, Mazumder J (2011) Feedback control of melt pool temperature during laser cladding process. *IEEE Trans Control Syst Technol* 19(6):1349–1356
- Spears TG, Gold SA (2016) In-process sensing in selective laser melting (SLM) additive manufacturing. *Integr Mater Manuf Innov* 5(1):2
- Verhaeghe F, Craeghs T, Heulens J, Pandelaers L (2009) A pragmatic model for selective laser melting with evaporation. *Acta Mater* 57(20):6006–6012
- Zhang P, von Freyberg A, Fischer A (2017) Closed-loop quality control system for laser chemical machining in metal micro-production. *Int J Adv Manuf Technol* 93(9–12):3693–3703

**Publisher's Note** Springer Nature remains neutral with regard to jurisdictional claims in published maps and institutional affiliations.